Medical Physics
The International Journal of Medical Physics Research and Practice

Analysis of the spatial-frequency-dependent DQE of optically coupled digital mammography detectors

Andrew D. A. Maidment and Martin J. Yaffe

Citation: Medical Physics **21**, 721 (1994); doi: 10.1118/1.597331
View online: http://dx.doi.org/10.1118/1.597331
View Table of Contents: http://scitation.aip.org/content/aapm/journal/medphys/21/6?ver=pdfcov
Published by the American Association of Physicists in Medicine

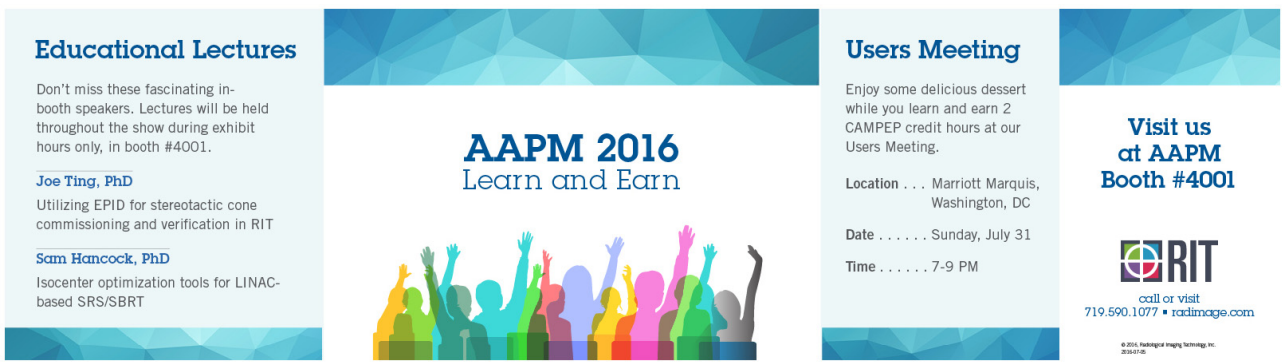

Analysis of the spatial-frequency-dependent DQE of optically coupled digital mammography detectors

Andrew D. A. Maidment[a] and Martin J. Yaffe
Departments of Medical Biophysics and Radiology, University of Toronto, and Research Division, Sunnybrook Health Science Centre, 2075 Bayview Avenue, Toronto, Ontario M4N 3M5 Canada

(Received 1 September 1993; accepted for publication 11 March 1994)

The effect of optical coupling efficiency on the spatial-frequency-dependent propagation of signal and noise is considered for x-ray image detectors for digital mammography in which a phosphor screen is optically coupled to a charge-coupled device (CCD) image array. For experimental purposes, optical coupling between a Gd_2O_2S:Tb phosphor screen and a CCD image array was provided by relay lenses. Neutral density filters were inserted between the lenses to vary the optical coupling efficiency without altering the inherent spatial resolution. The total coupling efficiency, defined as the number of electrons (e^-) recorded in the CCD per x-ray interaction in the phosphor, was calculated in each case. The modulation transfer function, and the contributions to the total noise power spectrum (NPS) of x-ray quantum noise, secondary quantum noise, and inherent detector noise were measured as a function of coupling efficiency. These data were used to calculate the spatial-frequency-dependent detective quantum efficiency [DQE(f)]. The NPS due to x-ray quantum noise had a significant spatial-frequency dependence for coupling efficiencies of more than 9 e^- per x-ray interaction, but little spatial-frequency dependence for coupling efficiencies of less than 2 e^- per x-ray interaction. These results indicate that to preserve high spatial-frequency values of DQE(f), and to ensure that images are x-ray quantum-noise limited at high spatial frequencies, a coupling efficiency on the order of 10 e^- per x-ray interaction is required. This is contrary to the common belief, based on zero spatial-frequency analysis, that a coupling efficiency on the order of 1 e^- per x-ray interaction is sufficient to acquire x-ray quantum-noise-limited images.

Key words: digital mammography, x-ray detector, optical coupling efficiency, modulation transfer function, noise power spectra, detective quantum efficiency

I. INTRODUCTION

We have developed a prototype of a scanned-slot digital mammography imaging system at the University of Toronto which is suitable for clinical use in terms of spatial resolution, contrast sensitivity, and image acquisition time.[1,2] The detector for this system, shown in Fig. 1, consists of a Gd_2O_2S:Tb phosphor screen fiber-optically coupled to time-delay integration charge-coupled device (CCD) image arrays. The optical coupling provides the necessary demagnification to match the desired pixel size at the phosphor screen to the CCD element size.

When designing a system with an optically coupled phosphor screen, care must be exercised to ensure that the Poisson-distributed fluctuation in the number of detected x-ray quanta is the dominant source of noise. In a previous work,[3] we considered the factors affecting the coupling efficiency of detectors in which a phosphor screen is optically coupled to a CCD. In this paper, we consider the effect of coupling efficiency on the modulation transfer function (MTF), the noise power spectrum (NPS), and the spatial-frequency-dependent detective quantum efficiency [DQE(f)] in such imaging systems.

The zero spatial-frequency analysis of the propagation of noise in radiological imaging systems is well understood.[4–6] Sturm and Morgan[4] were among the first to demonstrate that the statistical properties of the x-ray quanta must be preserved to ensure that all of the information contained in an image is recorded. In the optically coupled detector shown schematically in Fig. 2, the x-ray signal is first converted to light and then to electrons. On the basis of zero spatial-frequency analysis, the statistical fluctuation in the number of x-ray quanta is the dominant source of noise, if the mean number of secondary quanta (e.g., light quanta or electrons) per x-ray interaction is greater than unity at every stage in the imaging system.[5] Otherwise, a *secondary quantum sink* exists and the image signal-to-noise ratio is degraded.

A large number of digital radiographic or fluoroscopic imaging systems have been proposed or developed in which a phosphor screen is optically coupled to a photoelectronic detector.[7–13] In such systems, considerable attention should be given to avoiding a secondary quantum sink. Specifically, the gain or coupling efficiency of each stage must be sufficient to ensure that at no point in the imaging system does the number of secondary quanta per x-ray interaction fall below unity. A more practical interpretation of the effect of secondary quantum noise would require that the magnitude of the secondary quantum noise be reduced as much as possible. For example, Nishikawa and Yaffe[14] recommend that the minimum total coupling efficiency should be on the order of ten electrons per x-ray interaction.

In this paper, we present experimental measurements of the effect of coupling efficiency on the spatial-frequency dependent functions MTF, NPS, and DQE(f). These data allow one to demonstrate the increased zero spatial-frequency noise that results from decreased coupling efficiency. This is due to the decrease in the *magnitude* of the x-ray quantum noise relative to the secondary quantum noise, and results in

 0094-2405/94/21(6)/721/9/$1.20

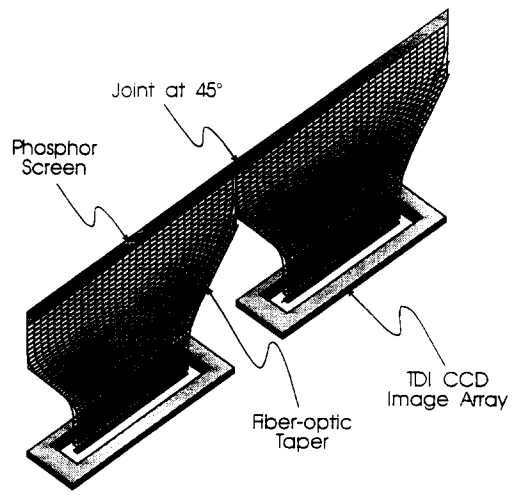

FIG. 1. Schematic of a prototype clinical scanned-slot digital mammography detector in which a phosphor is optically coupled to a CCD image array via a demagnifying fiber optic taper.

a drop in the DQE at zero spatial frequency. We also investigate the effect of coupling efficiency on the *shape* of the x-ray quantum noise power spectrum and the behavior of DQE(f) at high spatial frequencies.

II. THEORY

A. Zero spatial-frequency analysis

In the detector shown schematically in Fig. 2, x rays (which are Poisson distributed in both time and space) interact in a phosphor screen with a probability, A_Q, which is governed by binomial statistics. It is assumed that both the absorption of x-ray energy and the production of the resultant light quanta occur at a point. This is a reasonable assumption for a Gd_2O_2S phosphor for x rays with energy below the K edge of Gd (50.2 keV), such as those used in mammography, since, for example, the range [J. R. Cunningham (private communication, 1990)] of a 40-keV electron is only 5.5 μm. On average, $\bar{g}$ light quanta escape from the phosphor screen per x-ray interaction. The variation due to

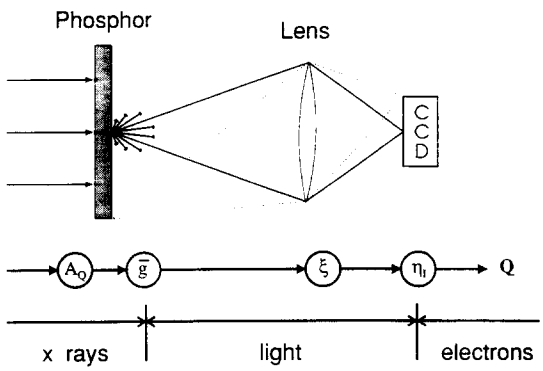

FIG. 2. Schematic of a detector in which a phosphor screen is optically coupled to a CCD. The statistical processes associated with each conversion step, the mean values, and the type of quanta connecting the steps are shown.

the statistical processes that govern the production and escape of light quanta is quantified by the Swank factor,[15,16] A_S. The emitted light quanta can then produce electrons in the CCD if (1) the light quanta are emitted within the acceptance solid angle of the lens (or other optical element); (2) they are transmitted through the optics; and (3) they generate an electron–hole pair in the CCD. The likelihood of each of these three steps occurring is governed by binomial probability distributions.

The DQE is defined as the square of the ratio of the signal-to-noise ratio (SNR) at the output of the detector to that at the input. As derived in the Appendix using the results of Albrecht,[5] the zero spatial-frequency DQE of an optically coupled detector without image intensification, is given by

$$\mathrm{DQE}=\frac{A_Q\bar{g}\xi\eta_I}{1+\bar{g}\xi\eta_I(1/A_S+1/\bar{g})}, \tag{1}$$

where ξ is the product of the optical coupling efficiencies of all intervening optical elements and η_I is the quantum efficiency of the CCD image array. A_Q, A_S, and $\bar{g}$ are as defined above. In the denominator, the first term describes the magnitude of the secondary quantum-noise relative to that of the x-ray quantum noise (the second term). This expression is valid in the absence of electronic noise sources.

For Gd_2O_2S:Tb phosphor irradiated with 20-keV x rays, 1350 light quanta will be produced, on average, per x-ray interaction.[17] Absorption of light in the screen and other losses will reduce the value of $\bar{g}$ to between 400 and 1000 light quanta, depending on the optical properties of the screen. For a detector with $A_S=1$ and $\bar{g}>100$, Eq. (1) can be simplified to the model of Barrett and Swindell,[18]

$$\mathrm{DQE}=\frac{A_Q}{1/C_T+1}, \tag{2}$$

where $C_T=\bar{g}\xi\eta_I$ is the total coupling efficiency in electrons per interacting x ray.

As a point of reference, the value $C_T=1$ (i.e., 50% drop in DQE) will be used to compare the results of various imaging systems. When C_T is less than unity, fewer than one secondary quantum per x ray will be recorded, a secondary quantum sink will occur, and the fluctuation in the number of secondary quanta will be the dominant source of noise. When C_T is greater than unity, the x-ray quantum noise will be dominant.

B. Spatial-frequency analysis

SNR and DQE can be expressed in terms of spatial frequencies. That is,

$$\mathrm{DQE}(f)=\frac{\mathrm{SNR}^2_{\mathrm{out}}(f)}{\mathrm{SNR}^2_{\mathrm{in}}(f)}. \tag{3}$$

This equation may be rearranged to separate the propagation of signal from the propagation of noise. The spatial-frequency dependence of the propagation of the signal is given by the MTF of the detector. The propagation of the noise is given by the ratio of $W_T(f)$, the output NPS, to the input NPS. The input NPS is independent of spatial frequency by virtue of the random spatial distribution of x rays[19] and the assumption that an x-ray interaction can be

localized to a region which is small relative to the resolution of the detector. The magnitude of the input NPS is determined by the x-ray quantum fluence, ϕ. The DQE(f) is given by[20]

$$\mathrm{DQE}(f)=\frac{\phi\kappa^2\mathrm{MTF}^2(f)}{W_T(f)}, \tag{4}$$

where κ is a constant that relates changes in incident fluence at zero spatial frequency to changes in detector output. This formulation is used to experimentally measure and calculate DQE(f), since each of the variables can be easily measured.

The total output NPS, $W_T(f)$, can be expressed as the sum of three constituent noise sources.[14] In this expression,

$$W_T(f)=W_Q(f)+W_{SQ}(f)+W_D(f). \tag{5}$$

All NPS are expressed in terms of electrons generated in the image array. Following the work of Barnes,[21] $W_Q(f)$ includes factors to describe both the fluctuation in the number of x-rays interacting in the screen and the variation in the number of light quanta emitted from the screen per x-ray interaction (i.e., A_S). $W_{SQ}(f)$ is due to the statistical fluctuation in the number of secondary quanta that would occur in the absence of x-ray quantum noise. Since each secondary quantum arises independently, these quanta are uncorrelated and $W_{SQ}(f)$ is spatial-frequency independent.[19] $W_D(f)$ is due to inherent detector output-signal fluctuations. Since $W_D(f)$ is caused by the random generation of electrons in the CCD readout process, it too should be spatial-frequency independent. A low inherent-noise detector is necessary in digital mammography to ensure x-ray quantum-noise-limited images.

For an ideal detector MTF(f)=1 at all frequencies and $W_Q(f)$ would be spatial-frequency independent, similar to the input x-ray NPS. But because of the optical quantum gain provided by the phosphor and the spatial spreading of light within the phosphor screen, light from each x-ray interaction is produced in bursts which are spatially correlated. High spatial frequency objects are represented by light bursts which are closely spaced and hence overlap causing image blurring. For this reason, high spatial-frequency signals are propagated and recorded with less modulation than low spatial-frequency signals. Lubberts has shown,[22] that as a first approximation, the shape of the light bursts (i.e., the spatial correlation) similarly affects the propagation of the noise. Hence $W_Q(f)$ will more closely match the input NPS at low spatial frequencies than at high spatial frequencies.

In an attempt to distinguish between the effects of x-ray quantum noise and other noise sources, Nishikawa and Yaffe[14,20,23] have factored DQE(f) as follows:

$$\mathrm{DQE}(f)=A_Q A_S R_C(f) R_N(f),$$

where

$$R_C(f)=\mathrm{MTF}^2(f)/\mathrm{NTF}_Q^2(f),$$

$$R_N(f)=W_Q(f)/W_T(f), \tag{6}$$

$$\mathrm{NTF}_Q^2(f)=W_Q(f)/W_Q(0).$$

Zero spatial-frequency effects of x-ray quantum noise are contained in the x-ray quantum detection efficiency, A_Q, and the Swank factor, A_S. $R_C(f)$ describes the relationship between the spatial-frequency dependence of the propagation of signal and noise. $\mathrm{NTF}_Q(f)$ is the noise analog of the modulation transfer function, thus $\mathrm{NTF}_Q^2(f)$ describes the spatial-frequency dependence of $W_Q(f)$, the x-ray quantum NPS. Finally, $R_N(f)$ is the ratio of the x-ray quantum noise power to the total noise power. This ratio describes the extent to which a detector is x-ray quantum-noise limited at each spatial frequency. Equation (6) is used, below, to investigate the spatial-frequency-dependent propagation of signal and noise, and to determine for which spatial frequencies a detector is x-ray quantum-noise limited.

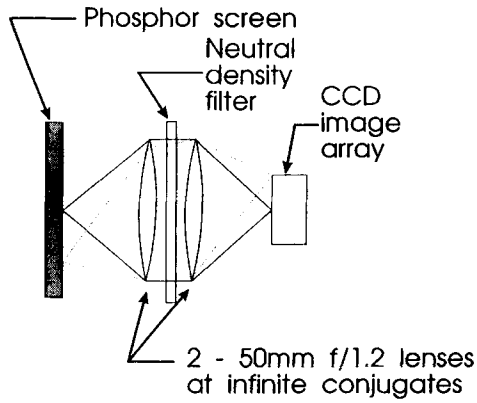

FIG. 3. The imaging system used for experiments. A Gd_2O_2S:Tb phosphor screen is coupled to a CCD image array via relay lenses. Neutral density filters may be inserted between the lenses.

III. EXPERIMENTAL PROCEDURE

The effect of coupling efficiency on MTF, NPS, and DQE(f) was measured with the imaging system shown in schematic in Fig. 3. The system consists of a 32 mg/cm^2 Gd_2O_2S:Tb phosphor screen coupled to a CCD image array via relay lenses. The optical coupling efficiency can be varied by inserting neutral density filters where the two 50 mm, $f/1.2$ lenses are focused at infinite conjugates. Five different coupling efficiencies were obtained using the neutral density filters listed in Table I. The CCD is a virtual-phase, frame-transfer device with 244×774 pixels of size 19.75 μm×8.5 μm. The camera design includes on-chip double correlated sampling, on-chip integration of charge, slow charge readout, and Peltier effect coolers to reduce the measured readout noise to 27 e^- at 5 °C. The CCD has a well capacity of

TABLE I. The optical density and percent transmission of the filters used. Also shown are the calculated number of x rays absorbed, the corresponding number of electrons produced, and the coupling efficiency.

OD of filter	Transmission (%)	X rays absorbed per pixel	e^- produced per pixel	e^- produced per x ray absorbed
0.0	100	1 550	26 400	17.0
0.3	50	3 000	27 300	9.1
0.7	20	7 900	26 200	3.3
1.0	10	14 500	26 500	1.8
1.3	5	29 700	26 400	0.9

86 000 e^-, giving a dynamic range of 3200:1. We measured that the CCD dark signal was generated at an average rate of 58 e^- pixel^{-1} s^{-1} at this temperature. An integration time of 1.000 s was used for the experiments.

In all experiments, the CCD signal was kept approximately constant. The experiments were designed to ensure that the neutral density filters did not alter the inherent resolution of the phosphor screen and CCD image array, or alter the focus of the lenses. This design ensured that variations in the spatial-frequency dependence of MTF, NPS, and DQE(f) were due to the variation in optical coupling efficiency and not due to the experimental apparatus.

In the experiments described, a tungsten target x-ray tube was used with a constant potential generator operated at 40 kV. The measured HVL of the x-ray beam was 0.88-mm of Al. To determine the contributions of secondary quantum noise, an integrating sphere and LED light source[24] were used to produce a signal in the CCD which was approximately equal to that obtained in the x-ray experiments. The light source simulates both the angular emission and light spectrum of the Gd_2O_2S:Tb phosphor used in the experiments. Dark signal measurements were obtained by operating the CCD in the same manner as above, but without illumination or x irradiation.

The number of x-ray quanta incident upon and interacting in the phosphor screen, and the phosphor screen interaction efficiency, A_Q, were calculated using an energy transport model.[25,26] The CCD camera was calibrated, in terms of electrons per unit digital signal, using the mean-variance technique.[27–29] This calibration allowed coupling efficiencies to be calculated in units of electrons (e^-) generated in the CCD per x-ray interaction in the screen.

All images were corrected for pixel-to-pixel variations in gain and offset, and a slight nonlinearity of the CCD image array. Correction factors were calculated for each experiment from 20 frames acquired with uniform illumination and from 50 frames acquired without illumination.[27] Multiple frames were acquired to reduce the uncertainty in the calculated correction factors.

A. MTF

Each MTF was determined from measurements of edge spread functions (ESF) provided by positioning a 0.4-mm thick tantalum plate with a polished edge between the x-ray tube and the phosphor screen. The tantalum obscured about one half of the field of view of the CCD. The edge was placed at about a 2° angle with respect to the columns of the CCD. In this way, images were formed which consisted of sets of ESFs, with 1 ESF per line. The ESF from each line was displaced 1/30 to 1/50 of a pixel with respect to the adjacent lines, depending upon the angle of the edge. Using the method of Judy,[30] the ESF sets were combined to yield a ten times oversampled ESF. This oversampled ESF was then numerically differentiated to obtain the line spread function (LSF), and the modulus of the Fourier transform of the normalized LSF was calculated to obtain the MTF. This method of calculating the MTF prevents aliasing and sampling errors due to the size, shape, and spacing of the detector elements.

B. NPS

The image data used to calculate the NPS, were acquired with the entire detector area uniformly irradiated. The NPS were calculated by employing the direct Fourier transform method.[20,31,32] Data were summed in one direction to synthesize the effect of a scanning slit 8.5-μm wide and 1.98-mm long. Each synthesized record contained 512 elements, allowing us to calculate spectral estimates for spatial frequencies between 0.23 and 58.8 mm^{-1}. It was found that synthesizing slits longer than 2 mm did not alter the shape of the calculated NPS, indicating that a good estimate of the central section of the 2-dimensional NPS had been obtained. To reduce random error in spectral estimates, 160 individual power spectra were measured and averaged. Corrections for the finite length and width of the synthetic aperture[33] allowed the true noise power spectra to be obtained.

In order to reduce the uncertainty of the spectral estimates, the spectral values of every five adjacent frequencies in the original spectra were binned (averaged) to generate the spectra presented. The zero spatial-frequency value was not included in the average. The spectral estimates are given in increments of 1.15 mm^{-1} and have a standard error[34] of 3.5%.

The secondary quantum noise, $W_{SQ}(f)$, and the dark noise, $W_D(f)$, were measured separately, but in the same fashion as $W_T(f)$. Since both spectra were found to be essentially frequency independent, within statistical errors, the spectral estimates were calculated as the average over the frequencies of interest (0 to 20 mm^{-1}). As a result of the averaging process, the spectral estimates of $W_{SQ}(f)$ and $W_D(f)$ have a standard error of 0.8%. $W_Q(f)$ was calculated by subtracting $W_D(f)$ and $W_{SQ}(f)$ from $W_T(f)$.

C. DQE(f)

DQE(f) were calculated using Eq. (4). To reduce statistical uncertainties in the estimates of DQE(f), 50 separate MTF measurements were averaged, and the values from every four adjacent frequencies were binned. The number of samples per frequency bin for the MTF and the NPS were chosen to ensure that the frequencies of the averaged functions occurred in the same increments. The resulting DQE(f) estimates have a standard error of 5%, arising mostly from the uncertainty in the NPS estimates.

IV. RESULTS

Listed in Table I are the optical density (OD) and the corresponding fractional transmission of the neutral density filters. In these experiments, the CCD signal was kept constant at approximately 26 500 electrons per pixel, regardless of optical coupling efficiency. Also shown in Table I, are the estimated number of x rays absorbed per pixel in the phosphor screen, the actual number of electrons recorded per pixel, and the calculated coupling efficiency in electrons per x ray. The maximum coupling efficiency was 17 and the minimum was 0.9 e^-/x ray. The estimates of coupling efficiency have an accuracy of about 2%. A systematic uncertainty in the number of x rays interacting in the phosphor exists, because of possible differences between the experi-

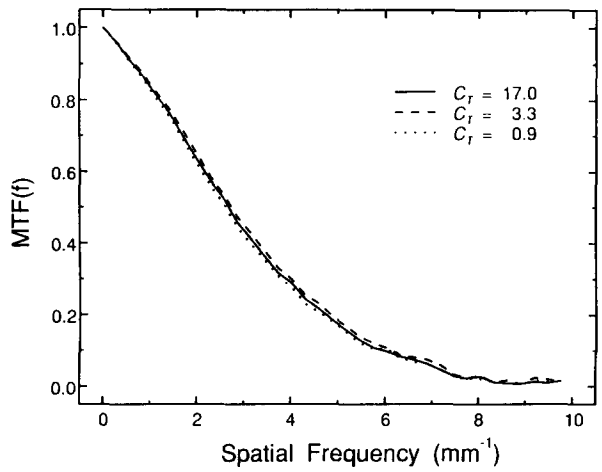

FIG. 4. The MTF of the imaging system without a neutral density filter yielding 17 e^-/x ray, and with two different filters yielding 3.3 and 0.9 e^-/x ray. Only three are shown to avoid confusion.

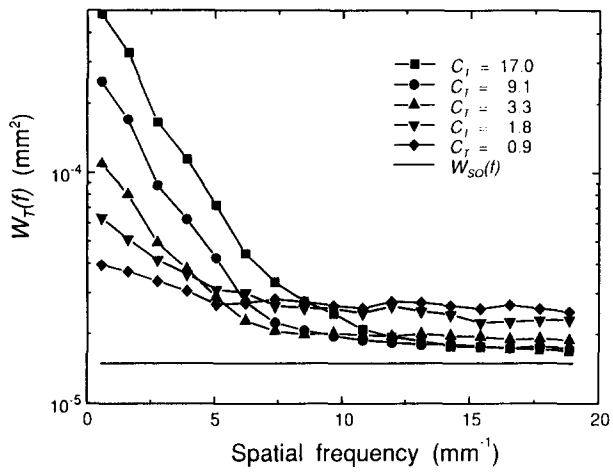

FIG. 6. The total NPS, $W_T(f)$, for detectors with five different coupling efficiencies from 17 to 0.9 e^-/x ray. Also shown is the NPS due to secondary quantum noise, $W_{SQ}(f)$.

mental x-ray spectra and those used in the energy transport model. However, even if differences as large as ±0.1 mm in HVL existed between the spectra, the variation in the mean energy absorbed in the screen would be less than ±10%.

Shown in Fig. 4 are the results of the MTF measurements of the experimental detector over the range of values of coupling efficiency, C_T. The data are indistinguishable within experimental error. The MTF^2 is shown in more detail in Fig. 7.

Shown in Fig. 5 are $W_T(f)$, $W_Q(f)$, $W_{SQ}(f)$, and $W_D(f)$ for the detector for a coupling efficiency of 17 e^-/x ray. In Fig. 6, the total NPS $[W_T(f)]$ for the five different coupling efficiencies are shown. Because the signal in the CCD was kept nearly constant, the magnitude of the secondary quantum noise and the dark noise did not vary significantly between experiments. In Fig. 7 the MTF$^2(f)$ and NTF$_Q^2(f)$ are compared.

In Fig. 8, the values of DQE(0) for the five coupling efficiencies are shown and are compared to the model representing the zero spatial-frequency values of the DQE given by Eq. (1). In the calculation of DQE(0), we used an x-ray spectrum-weighted[25] value of $A_Q=0.49$, and measured values[16] of $\bar{g}=470$ and $A_S=0.73$. In Fig. 9, the DQE(f) for the five coupling efficiencies are shown. Note that the high spatial-frequency values decrease more rapidly for detectors with poor coupling efficiency as compared to the detector with higher coupling efficiency.

Using Eq. (6), A_QA_S, $R_C(f)$, and $R_N(f)$ were calculated from the above values of $W_Q(f)$, $W_T(f)$, and MTF(f). In Fig. 10 $R_C(f)$ are presented, and in Fig. 11 $R_N(f)$ are presented. The zero frequency term $A_QA_S=0.36\pm0.02$. This is in agreement with our calculated values of A_Q and with previously measured[16] values of $A_S=0.73$.

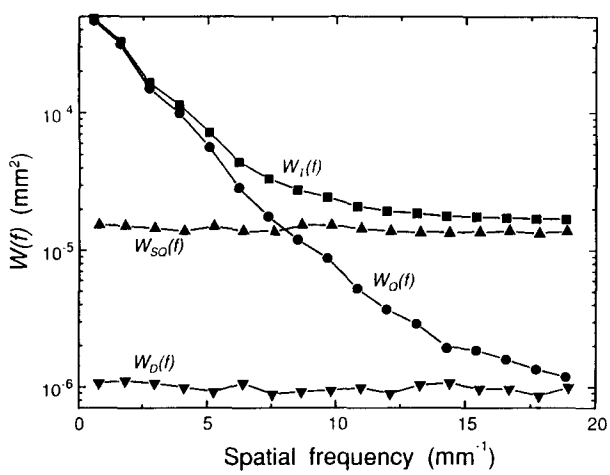

FIG. 5. The total NPS $[W_T(f)]$, and that due to x-ray quanta $[W_Q(f)]$, secondary quanta $[W_{SQ}(f)]$ and detector noise $[W_D(f)]$, measured using a coupling efficiency of $C_T=17$ e^-/x ray.

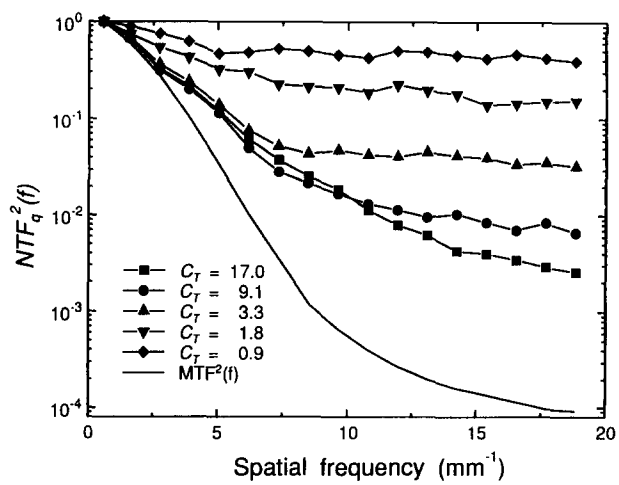

FIG. 7. The quantum noise transfer function, NTF$_Q^2(f)$, for detectors with five different coupling efficiencies. MTF$^2(f)$ is shown for comparison.

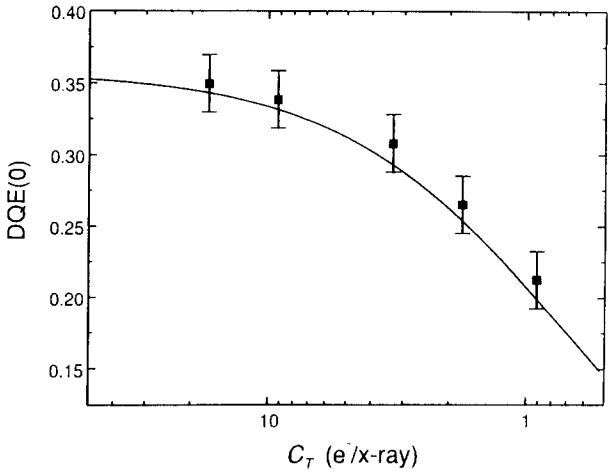

FIG. 8. Experimentally measured values of zero spatial-frequency detective quantum efficiency plotted for values of C_T. The solid line is given by Eq. (1), assuming A_Q=0.49, and A_S=0.73.

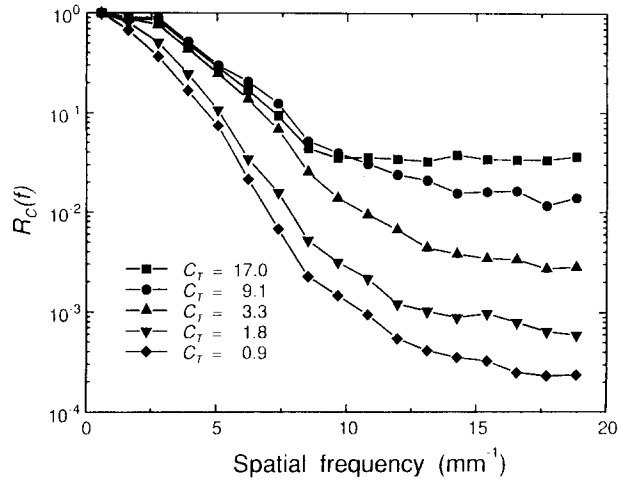

FIG. 10. Plot of $R_C(f)$ as a function of spatial frequency for various coupling efficiencies. The data points are connected with straight lines to aid the reader.

V. DISCUSSION

A. MTF(f)

The experiments, described above, were designed to measure the effect of total coupling efficiency, C_T, on the MTF, NPS, and DQE(f) for an imaging system in which a phosphor screen is optically coupled to a CCD image array. To facilitate experimental measurements, a lens-coupled detector was used, however, the results are equally applicable to our clinical detector built with fiber optics.[2] The effect of coupling efficiency on the resolution or MTF of a lens-coupled detector is illustrated in Fig. 12. In a detector with good coupling efficiency (left), the point spread function (PSF) from each x-ray interaction will be statistically well represented by electrons in the CCD. In a detector with poor coupling efficiency (right), the PSF from each x-ray interaction will be represented by only a few electrons. Because of the random nature by which light and electrons propagate through the imaging system, the individual locations of the recorded electrons will vary from one x-ray interaction to another. However, the processes which govern the scattering (i.e., spreading) of light quanta from their point of origin in the phosphor screen do not change as a function of coupling efficiency. Therefore, the ensemble average of the PSFs (and hence the MTF) will not change as a function of coupling efficiency. This is confirmed by the results shown in Fig. 4.

B. NPS(f)

Since the shape of the MTF does not change with coupling efficiency, one might reason that the shape of the x-ray quantum NPS, $W_Q(f)$, would not change either. However, referring to Fig. 7, it is clear that $W_Q(f)$ *does* change with coupling efficiency. At low spatial frequencies and high coupling efficiencies $\mathrm{NTF}_Q^2(f)$ has a similar shape to $\mathrm{MTF}^2(f)$. At higher spatial frequencies $\mathrm{NTF}_Q^2(f)$ diverges from $\mathrm{MTF}^2(f)$ as predicted by Lubberts.[22] Note, however, that the

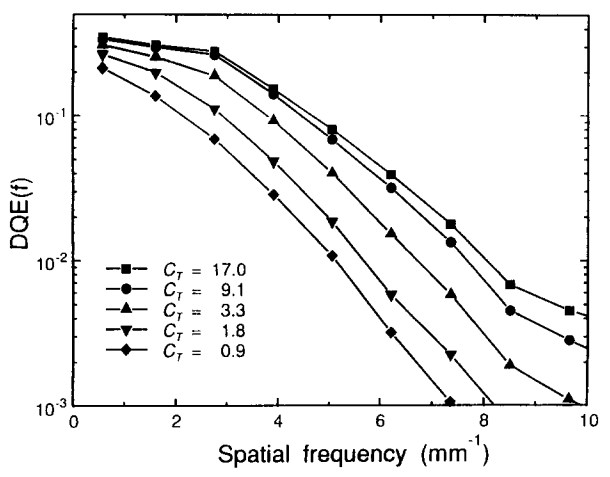

FIG. 9. Detective quantum efficiency plotted as a function of spatial frequency for detectors with five different coupling efficiencies.

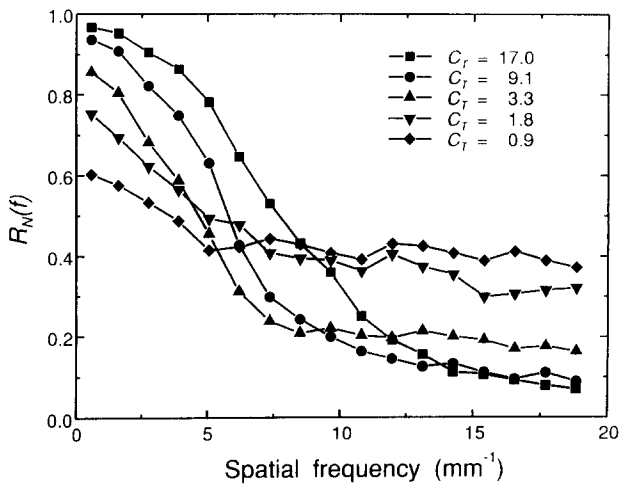

FIG. 11. Plot of $R_N(f)$ as a function of spatial frequency for various coupling efficiencies. The data points are connected with straight lines to aid the reader.

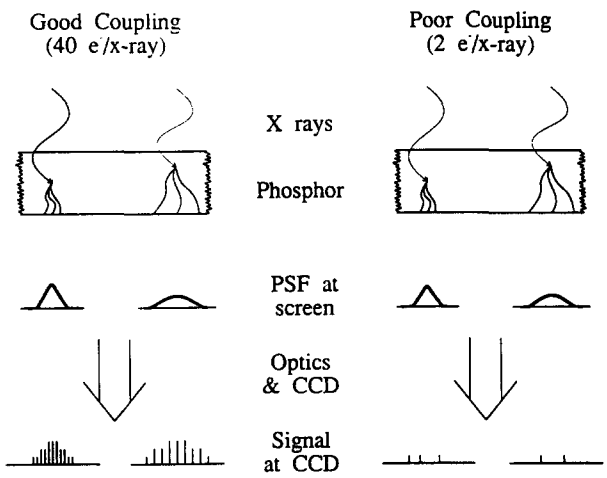

FIG. 12. Schematic illustrating how the optical PSF might be recorded in the CCD for two detectors; one with a coupling efficiency of 40 e^-/x ray (left) and the other with a coupling efficiency of 2 e^-/x ray.

frequency at which $NTF_Q^2(f)$ diverges from $MTF^2(f)$ decreases with decreasing coupling efficiency and the amount of divergence increases.

The effect of coupling efficiency on the propagation of noise is illustrated in Fig. 13. In this illustration, detectors with good (left), and poor (right) coupling efficiencies are again compared. X rays which interact in the phosphor screen (a), produce a spatial distribution of electrons in the CCD (b) after passing through the intervening optics. The autocorrelation function (ACF) of the distribution of electrons recorded in the detector (c) with good coupling efficiency demonstrates significant correlation, even for a moderate spatial shift, because each x-ray interaction produces a burst of many spatially correlated light quanta giving rise to a burst of many electrons in the CCD. The ACF of the spatial distribution of the electrons recorded by the detector with poor coupling demonstrates poor correlation because each x-ray interaction produces a burst of only a few electrons. Because of the shape of the ACF, its Fourier transform, the total NPS (d) measured with the detector exhibiting good coupling falls more quickly with spatial frequency than that of the detector exhibiting poor coupling efficiency.

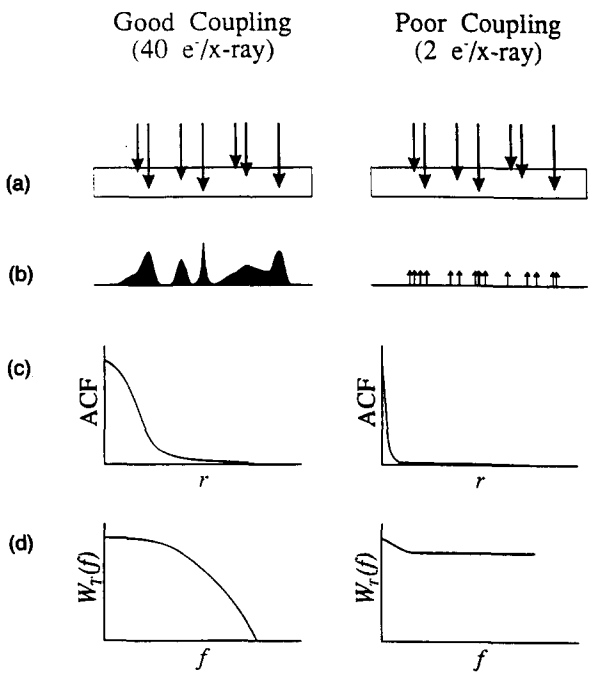

FIG. 13. Schematic illustrating how the random distribution of x rays (a), generates a group of PSFs which are recorded in the CCD (b). With a coupling efficiency of 40 e^-/x ray (left), the recorded PSFs each have significant correlation as illustrated by the autocorrelation function (ACF) shown in (c). Less correlation exists for the detector with a coupling efficiency of 2 e^-/x ray (right). The corresponding NPS are illustrated in (d).

Current theories of the propagation of x-ray quantum noise[14,23,35–38] do not account for the relationship between coupling efficiency and the shape of $W_Q(f)$, although the concept that the correlation present in secondary quanta of individual x-ray interactions may be used to derive the NPS has been explained previously.[39,40]

The key difference between the MTF measurement and the NPS measurement, is that when measuring the MTF, the spatial distribution of x rays is well defined by nature of the measuring apparatus, thus, correlation between PSFs is maintained. When these PSFs are superposed in the MTF experiment, the averaging process will produce the same edge spread function for either good or poor coupling. However, when measuring the NPS, the spatial distribution of the x rays is random and only the correlation provided by the recorded secondary quanta can be measured. By decreasing the coupling efficiency, that correlation is reduced.

C. DQE(*f*)

The effect of coupling efficiency on DQE(f) is twofold. First, as predicted by the zero spatial-frequency analysis [Eq. (1)] and by $R_N(0)$ (see Fig. 8), the zero spatial-frequency value of DQE(f) decreases with decreasing coupling efficiency. The reduction in the DQE(0) is due to the reduction of the *magnitude* of $W_Q(0)$ relative to $W_{SQ}(0)$ and $W_D(0)$.

The second effect is related to the frequency dependence (*shape*) of $W_Q(f)$ relative to $W_{SQ}(f)$ and $W_D(f)$. If the shape of $W_Q(f)$ did not vary with coupling efficiency, then the reduction in DQE(f) at high spatial frequencies would be similar to that which occurs at zero spatial frequency. However, the shape of $W_Q(f)$ does change with coupling efficiency causing DQE(f) to decrease more quickly as a function of coupling efficiency at high spatial frequencies. Zero spatial-frequency analysis of DQE will underestimate the effect of coupling efficiency on high spatial-frequency DQE. Thus while a detector may be x-ray quantum-noise limited at low spatial frequencies, the same may not be true at high spatial frequencies.

The spatial-frequency dependence of DQE(f), which is dependent upon both MTF and $W_T(f)$, will vary less with coupling efficiency than predicted by $W_Q(f)$ alone. The effect on DQE(f) of $W_Q(f)$ is given by $R_C(f)$, and is shown in Fig. 10. As C_T decreases, $W_Q(f)$ demonstrates less frequency dependence because there is less correlation between electrons in the burst from each x-ray interaction. $R_C(f)$ most clearly demonstrates the changing correlation between

MTF(f) and $W_Q(f)$. Note that as coupling efficiency decreases, the value of $R_C(f)$ drops dramatically.

In the calculation of DQE(f), the relative magnitudes and shapes of the x-ray quantum noise are compared to the total NPS by $R_N(f)$, which is shown in Fig. 11. The frequency dependence of $W_Q(f)$ decreases more significantly with decreasing coupling efficiency than does $W_T(f)$ due to the influence of the frequency-independent additive noise sources $W_{SQ}(f)$ and $W_D(f)$. As a result, $R_N(f)$ loses its spatial frequency dependence with decreasing values of C_T, because both $W_{SQ}(f)$ and $W_D(f)$, which appear in the denominator of the expression for $R_N(f)$, are also spatial-frequency independent. Hence over the range of values of C_T which we examined, low frequency values of $R_N(f)$ decreased with decreasing coupling efficiency while the high-frequency values of $R_N(f)$ increased slightly because of the higher quantum noise transfer (Fig. 7) seen with reduced C_T. The result is that for low C_T, the product $R_C(f)R_N(f)$ is a more slowly decreasing function of spatial frequency than is $R_C(f)$ alone.

The coupling efficiency has the greatest effect upon the shape of the DQE(f) for C_T in the range of 1 to 10 e^-/x ray. Doubling the coupling efficiency from 9 to 17 e^-/x ray did not significantly affect the shape of $W_Q(f)$ (see Fig. 7). This would suggest, therefore, that C_T on the order of 10 e^-/x ray should be treated as the minimum value appropriate for high resolution imaging systems in which a phosphor screen is optically coupled to a CCD image array. However, even though the shape of $W_Q(f)$ did not change significantly between C_T=9 and C_T=17, the magnitude of $W_Q(f)$ relative to $W_{SQ}(f)+W_D(f)$ increased by factor of 2. Therefore, one should choose a coupling efficiency which guarantees that the detector is x-ray quantum-noise limited at all spatial frequencies of interest in the detection of radiographically significant objects, and in general, the maximum possible coupling efficiency that does not exceed the dynamic range capability of the detector should be used.

VI. CONCLUSIONS

As coupling efficiency is reduced, two effects occur. First, the DQE is reduced at low spatial frequencies because the magnitude of the secondary quantum noise is increased relative to the x-ray quantum noise. Second, the DQE(f) decreases more rapidly with increasing spatial frequency. Therefore, the decrease in DQE(f) as a function of coupling efficiency is more significant at high spatial frequencies. This decrease is the result of the loss of correlation between the propagation of signal and noise [i.e., $R_C(f)$ decreases with decreased coupling efficiency]. However, because of the presence of secondary quantum noise and inherent detector noise which increase $W_T(f)$ uniformly at all spatial frequencies, the decrease in DQE(f) is less dramatic than predicted by $R_C(f)$ alone.

Current methods used to determine the minimum required coupling efficiency to obtain x-ray quantum-noise limited images are based on zero-spatial frequency analyses. These methods underestimate the coupling efficiency required, indicating that on the order of 1 e^-/x ray is required to ensure that the x-ray quantum noise is dominant. In this paper, we have demonstrated that a coupling efficiency on the order of 10 e^-/x ray is required to ensure that a detector is x-ray quantum-noise limited at high spatial frequencies. In addition, we recommend that the maximum practical coupling efficiency be used, but in any case, C_T should be sufficiently high to ensure $R_N(f)>0.5$ for all spatial frequencies of interest.

ACKNOWLEDGMENTS

The authors would like to thank Dr. J. A. Rowlands, Dr. R. M. Nishikawa of the University of Chicago, Dr. R. VanMetter of the Eastman Kodak Research Laboratory, and Mr. D. Mah for many helpful discussions. This work is supported by the Medical Research Council of Canada, and the National Cancer Institute of Canada. The first author is the recipient of a University of Toronto Open Doctoral Fellowship. Presented in part at the Young Investigators Symposium 34th Annual Meeting of the AAPM, Calgary, August 24, 1992.

APPENDIX: DERIVATION OF EQ. (1)

Albrecht[5] has shown that for an n-stage cascaded imaging system the mean value of the output signal, $\bar{Q}$, can be given by

$$\bar{Q}=\prod_{i=0}^{n}\overline{\alpha_i}, \tag{A1}$$

where $\overline{\alpha_0}$ is the mean number of quanta arriving per unit time, and $\overline{\alpha_1}$ to $\overline{\alpha_n}$ are the mean multiplicative factors for the n stages. The noise amplitude, $\sigma(Q)$, is defined as the standard deviation of Q, which may be calculated using

$$\sigma^2(Q)=\overline{Q^2}-\bar{Q}^2, \tag{A2}$$

where $\overline{Q^2}$ is the mean squared value of Q. Albrecht[5] has shown that

$$\sigma^2(Q)=\left[\prod_{i=0}^{n}\overline{\alpha_i}\right]\left[1-\prod_{j=0}^{n}\overline{\alpha_j}+\sum_{k=0}^{n}\left(\frac{\overline{\alpha_k^2}}{\overline{\alpha_k^2}}+\frac{1}{\overline{\alpha_k}}\right)\prod_{l=k}^{n}\overline{\alpha_l}\right]. \tag{A3}$$

In an optically coupled imaging system, α_0 is a random variable (RV) representing the number of x-ray quanta incident upon the phosphor screen, α_1 is a RV representing the fraction of x rays incident upon the phosphor screen which will be attenuated, α_2 is a RV giving the light gain of the phosphor screen (as measured at the output surface of the screen), α_3 to α_{n-1} are RVs which give the fraction of light successfully passing through the intervening optics, and α_n is a RV giving the fraction of light quanta incident upon the CCD which generate an electron–hole pair in the CCD image array. These processes may be divided into three separate groups. α_0 is represented by a Poisson distribution, α_2 is screen dependent, and all other stages are governed by binomial distributions. For a Poisson process, $\overline{\alpha_k^2}=\overline{\alpha}_k^2+\overline{\alpha}_k$, while for a binomial process $\overline{\alpha_k^2}=\overline{\alpha}_k$. For a fluorescent screen, Swank has defined $A_S=\overline{\alpha}_k^2/\overline{\alpha_k^2}$, where here the A_S notation of Rowlands *et al.*[41] is used. Thus

TABLE II. The stages, processes, governing statistical distributions, and their mean and mean square values.

Symbol	Process	Statistical distribution	$\overline{\alpha_k}$	$\overline{\alpha_k^2}$
α_0	Incident x-ray quanta	Poisson	I	I^2+I
α_1	Absorption of x-ray quanta	Binomial	A_Q	A_Q
α_2	Optical gain of phosphor screen	Screen dependent	$\bar{g}$	$\bar{g}^2/A_S$
α_4	Optical transmission efficiency	Binomial	ξ	ξ
α_5	CCD conversion efficiency	Binomial	η_I	η_I

$$\left(\frac{\overline{\alpha_k^2}}{\overline{\alpha_k^2}}-\frac{1}{\overline{\alpha_k}}\right)=\left(\frac{1}{A_S}-\frac{1}{g}\right), \quad \text{for phosphor screen,}$$

$$=1 \quad \text{if Poisson,}$$

$$=0 \quad \text{if binomial.}$$

The detective quantum efficiency (DQE) is the square of the ratio of the output SNR to the input SNR. The output SNR is given by $\bar{Q}/\sigma(Q)$. The input SNR is simply $\alpha_0^{1/2}$. In this way, the DQE may be calculated.

Consider, now, the four-stage imaging system in Fig. 2. The mean and mean square values of the RVs α_i are as listed in Table II. The DQE of the optically coupled system is, therefore,

$$\mathrm{DQE}=\frac{A_Q\bar{g}\xi\eta_I}{1+\bar{g}\xi\eta_I(1/A_S+1/\bar{g})}. \tag{A4}$$

In a system with a series of optical elements, the total coupling efficiency of the optics, ξ, is given by the product of the optical coupling efficiencies of all intervening optical elements.

[a]Current address: Department of Radiology, Thomas Jefferson University, 3390 Gibbon Building, 111 South 11th Street, Philadelphia, PA 19107-5098.

[1]A. D. A. Maidment, B. G. Starkoski, I. C. Soutar, G. E. Mawdsley, D. B. Plewes, and M. J. Yaffe, "A clinical scanned-slot digital mammography prototype," Radiology **185**(P), 249 (1992).

[2]A. D. A. Maidment, M. J. Yaffe, D. B. Plewes, G. E. Mawdsley, I. C. Soutar, and B. G. Starkoski, "Imaging performance of a prototype scanned-slot digital mammography system," Proc. SPIE **1896**, 93–103 (1993).

[3]A. D. A. Maidment, Ph.D. dissertation (University of Toronto, 1993).

[4]R. E. Sturm and R. H. Morgan, "Screen intensification systems and their limitations," Am. J. Roentgenol. Radium Ther. **62**(5), 617–634 (1949).

[5]C. Albrecht, "Noise Sources in Image Intensifying Devices," in *Diagnostic Radiological Instrumentation: Modulation Transfer Function,* edited by R. D. Moseley and J. H. Rust (Charles C. Thomas, Springfield, 1965), Chap. XVII.

[6]M. J. Yaffe and R. M. Nishikawa, "X-ray Imaging Concepts: Noise, SNR and DQE," in *Specification, Acceptance Testing, and Quality Control of Diagnostic X-ray Imaging Equipment,* edited by J. A. Seibert, G. T. Barnes, and R. G. Gould (AAPM Summer School, Santa Cruz, July 1991).

[7]R. H. Morgan and R. E. Sturm, "The Johns Hopkins fluoroscopic screen intensifier," Radiology **57**, 556–560 (1951).

[8]R. B. Holmes and D. J. Wright, "Image orthicon fluoroscopy of a 12-inch field and direct recording of the monitor image," Radiology **79**, 740–751 (1962).

[9]R. S. Nelson, Z. L. Barbaric, A. S. Gomes, C. L. Moler, and M. E. Deckard, "An evaluation of a fluorescent screen-isocon camera system for x-ray imaging in radiology," Med. Phys. **9**, 777–783 (1982).

[10]D. Sashin, D. Gur, C. W. Morris, and J. L. Ricci, "Isocon imaging for x-ray diagnostics," Proc. SPIE **78**, 108–112 (1976).

[11]S. Fritz, "Scanned projection radiography using a time-delay-and-integrate scanning CCD," Proc. SPIE **1090**, 330–338 (1989).

[12]H. Liu and A. Karellas, "Optical collection efficiency considerations in radiological imaging systems using lens coupling," Med. Phys. **19**, 847 (1992).

[13]M. J. M. Beerlage, H. P. L. Levels, and H. Mulder, "Digital slot radiography based on a linear x-ray image intensifier and two-dimensional image sensors," Proc. SPIE **626**, 161–169 (1986).

[14]R. M. Nishikawa and M. J. Yaffe, "Effect of various noise sources on the detective quantum efficiency of phosphor screens," Med. Phys. **17**, 887–893 (1990).

[15]R. K. Swank, "Absorption and noise in x-ray phosphors," J. Appl. Phys. **45**, 4109–4203 (1974).

[16]C. E. Dick and J. W. Motz, "Utilization of monoenergetic x-ray beams to examine the properties of radiographic intensifying screens," IEEE Trans. Nucl. Sci. **NS-28**, 1554–1558 (1981).

[17]R. A. Buchanon, "An improved x-ray intensifying screen," IEEE Trans. Nucl. Sci. **NS-19**, 81–86 (1972).

[18]H. H. Barrett and W. Swindell, *Radiological Imaging,* Vol. 1 (Academic, New York, 1981), pp. 287–289.

[19]J. C. Dainty and R. Shaw, *Image Science* (Academic, New York, 1974), p. 312.

[20]R. M. Nishikawa, G. E. Mawdsley, A. Fenster, and M. J. Yaffe, "Scanned-slot digital mammography," Med. Phys. **14**, 717–727 (1987).

[21]G. T. Barnes, "Radiographic mottle: A comprehensive theory," Med. Phys. **9**, 656–667 (1982).

[22]G. Lubberts, "Random noise produced by x-ray fluorescent screens," J. Opt. Soc. Am. **58**, 1475–1483 (1968).

[23]R. M. Nishikawa and M. J. Yaffe, "Model of the spatial frequency dependent detective quantum efficiency of phosphor screens," Med. Phys. **17**, 894–904 (1990).

[24]J. A. Rowlands, K. S. Schulenburg, and G. DeCrescenzo, "A light source for testing radiological television cameras," Med. Phys. **16**, 1–6 (1989).

[25]A. D. A. Maidment, R. Fahrig, and M. J. Yaffe, "Dynamic range requirements in digital mammography," Med. Phys. **20**, 1621–1633 (1993).

[26]R. Fahrig, A. D. A. Maidment, and M. J. Yaffe, "Optimization of peak kilovoltage and spectral shape for digital mammography," Proc. SPIE **1651**, 74–83 (1992).

[27]A. D. A. Maidment and M. J. Yaffe, "Scanned-slot digital mammography," Proc. SPIE **1231**, 316–326 (1990).

[28]L. Mortara and A. Fowler, "Evaluations of charge-couple device (CCD) performance for astronomical use," Proc. SPIE **290**, 28–33 (1981).

[29]G. R. Sims and M. B. Denton, "Characterization of a charge-injection-device camera system as a multichannel spectroscopic detector," Opt. Eng. **26**, 1008–1019 (1987).

[30]P. F. Judy, "The line spread function and modulation transfer function of a computed tomographic scanner," Med. Phys. **3**, 233–236 (1976).

[31]R. F. Wagner, "Fast Fourier digital quantum mottle analysis with application to rare earth intensifying screens," Med. Phys. **4**, 157–162 (1977).

[32]J. C. Dainty and R. Shaw, *Image Science* (Academic, New York, 1974), Chaps. 6 and 8.

[33]J. C. Dainty and R. Shaw, *Image Science* (Academic, New York, 1974), pp. 277–280.

[34]J. S. Bendat and A. G. Piersol, *Random Data,* 2nd ed. (Wiley, New York, 1986), pp. 278–286 and 393–404.

[35]T. Y. Fu, Ph.D. dissertation (University of Arizona, 1984).

[36]M. Rabbani, R. Shaw, and R. VanMetter, "Detective quantum efficiency of imaging systems with amplifying and scattering mechanisms," J. Opt. Soc. Am. A **4**, 895–901 (1987).

[37]M. Rabbani and R. VanMetter, "Analysis of signal and noise propagation for several imaging mechanisms," J. Opt. Soc. Am. A **6**, 1156–1164 (1989).

[38]R. VanMetter and M. Rabbani, "An application of multivariate moment-generating function to the analysis of signal and noise propagation in radiographic screen-film systems," Med. Phys. **17**, 65–71 (1990).

[39]J. A. Rowlands, K. W. Taylor, and H. N. Cardinal, "Imaging and noise limitations of cesium iodide x-ray image intensifiers," Proc. SPIE **454**, 366–376 (1984).

[40]M. Drangova and J. A. Rowlands, "Measurement of the spatial Wiener spectrum of nonstorage imaging devices," Med. Phys. **15**, 151–157 (1988).

[41]J. A. Rowlands and K. W. Taylor, "Absorption and noise in cesium iodide x-ray image intensifiers," Med. Phys. **10**, 786–795 (1983).